Rational Design of Novel Antimicrobials: Blocking Purine Salvage in a Parasitic Protozoan[†]

John R. Somoza,[‡,§] A. Geoffrey Skillman, Jr.,[§,||] Narsimha R. Munagala,[||] C. M. Oshiro,[||] Ronald M. A. Knegtel,[⊥] Solomon Mpoke,[||] Robert J. Fletterick,[‡] Irwin D. Kuntz,[||] and Ching C. Wang*,[||]

Department of Biochemistry and Biophysics, University of California, San Francisco, California 94143-0448, Department of Pharmaceutical Chemistry, University of California, San Francisco, California 94143-0446, and N. V. Organon, P.O. Box 20, 5340 BH Oss, The Netherlands

ABSTRACT: All parasitic protozoa obtain purine nucleotides solely by salvaging purine bases and/or nucleosides from their host. This observation suggests that inhibiting purine salvage may be a good way of killing these organisms. To explore this idea, we attempted to block the purine salvage pathway of the parasitic protozoan *Tritrichomonas foetus*. *T. foetus* is a good organism to study because its purine salvage depends primarily on a single enzyme, hypoxanthine−guanine−xanthine phosphoribosyltransferase (HGXPRTase), and could provide a good model for rational drug design through specific enzyme inhibition. Guided by the crystal structure of *T. foetus* HGXPRTase, we used structure-based drug design to identify several non-purine compounds that inhibited this enzyme without any detectable effect on human HGPRTase. One of these compounds, 4-[*N*-(3,4-dichlorophenyl)carbamoyl]phthalic anhydride (referred to as TF1), was selected for further characterization. TF1 was shown to be a competitive inhibitor of *T. foetus* HGXPRTase with respect to both guanine (in the forward reaction; $K_i = 13\ \mu$M) and GMP (in the reverse reaction; $K_i = 10\ \mu$M), but showed no effect on the homologous human enzyme at concentrations of up to 1 mM. TF1 inhibited the in vitro growth of *T. foetus* with an EC_{50} of approximately 40 μM. This inhibitory effect was associated with a decrease in the incorporation of exogenous guanine into nucleic acids, and could be reversed by supplementing the growth medium with excess exogenous hypoxanthine or guanine. Thus, rationally targeting an essential enzyme in a parasitic organism has yielded specific enzyme inhibitors capable of suppressing that parasite's growth.

Many pathogenic microorganisms are dependent on their hosts for key metabolites, and it should be possible to exploit this dependency for the design of novel chemotherapeutic agents. For example, all of the parasitic protozoa (e.g. Plasmodium, Toxoplasma, Leishmania, Trypanosoma, etc.) lack the ability to synthesize purine nucleotides de novo (*1*). Instead, these organisms rely on salvage enzymes to obtain purine bases and nucleosides from their host and convert them to the corresponding nucleotides. Thus, interfering with purine salvage could be an effective way of killing these organisms.

We sought to demonstrate the feasibility of this approach by blocking purine salvage in the parasitic protozoan *Tritrichomonas foetus*, an organism that can cause embryonic death and infertility in cows (*2*). *T. foetus* is a good model system because its purine salvage pathway is well understood and relies primarily on a single enzyme, hypoxanthine−guanine−xanthine phosphoribosyltransferase (HGXPRTase[1]), to replenish its purine nucleotide pool (*3*). HGXPRTase catalyzes the transfer of the ribose 5-phosphate moiety of α-D-5-phosphoribosyl-1-pyrophosphate (PRPP) to N9 of hypoxanthine, guanine, or xanthine to form the corresponding ribonucleotide.

Although mammals can produce purine nucleotides de novo, they also make use of purine salvage pathways. This is an important caveat to the idea of targeting purine salvage for chemotherapeutic purposes, because mammals recycle hypoxanthine and guanine using hypoxanthine−guanine phosphoribosyltransferase (HGPRTase), an enzyme that shares 27% sequence identity with tritrichomonal HGX-PRTase (*4*). Since a decrease in human HGPRTase activity can lead to hyperuricemia (*5*), it is important to block the pathogen's purine salvage pathway while leaving the corresponding mammalian pathway untouched.

Our goal was to selectively inhibit the *T. foetus* HGX-PRTase. This should block the main route of purine salvage, thus leading to growth arrest of the parasite. The only known

* To whom correspondence should be addressed: Department of Pharmaceutical Chemistry, UCSF, 513 Parnassus Ave., San Francisco, CA 94143-0446. Telephone: (415) 476-1321. Fax: (415) 476-3382. E-mail: ccwang@cgl.ucsf.edu.
[‡] Department of Biochemistry and Biophysics, University of California.
[§] These authors made equal contributions to this publication.
[||] Department of Pharmaceutical Chemistry, University of California.
[⊥] N. V. Organon.

[1] Abbreviations: HGXPRTase, hypoxanthine−guanine−xanthine phosphoribosyltransferase; PRPP, α-D-5-phosphoribosyl-1-pyrophosphate; PP$_i$, pyrophosphate; DMSO, dimethyl sulfoxide; ACD, Available Chemicals Directory.

inhibitors of the purine PRTases at present are purine analogues, and they are weak inhibitors with K_i values in the millimolar range (*6*). We decided that the most pragmatic strategy for identifying novel inhibitors of *T. foetus* HGX-PRTase would be to use the three-dimensional structure of this enzyme to guide our search. Furthermore, since the structure of the human HGPRTase has also been determined (*7*), this structure-driven approach should make it easier to identify compounds that selectively inhibit the parasite enzyme.

MATERIALS AND METHODS

Structure Analysis. The crystal structure of the *T. foetus* HGXPRTase was determined by Somoza et al. (*8*) at 1.9 Å resolution (PDB accession code 1HGX), and the crystal structure of the human HGPRTase was determined by Eads et al. (*7*) at 2.5 Å resolution (PDB accession code 1HMP). The software packages O (*9*), Insight II (*10*), MIDAS PLUS (*11*, *30*), Sybyl (*12*), and GEM (E. Fauman, unpublished work) were used for the display and analysis of the structures.

Docking. DOCK 3.5 (*13*−*15*) was used to screen the Available Chemicals Directory (ACD) for potential HGX-PRTase inhibitors (*16*). The docking process includes four primary tasks: (a) creating a negative image of the putative binding site, (b) overlaying the negative image with small molecules from a database, (c) scoring many orientations of a molecule on the basis of its complementarity to the protein, and (d) ranking and reviewing the best scoring orientations of the most complementary small molecules. The docking protocol applied to this particular study was modified from the general method in the following manner. First, chemical compounds were segregated into small, medium, and large size categories on the basis of the number of heavy atoms in each compound (small, 10−20; medium, 21−29; and large, 30−60). Matching and docking parameters were adjusted for each group of chemicals to achieve similar sampling of the binding site. Second, instead of it being a negative image of the entire active site, the negative image was limited to the region of the active site that interacts with the bound guanine and proximal part of the ribose, and to parts of the active site that differ between the parasite and human enzymes (total number of spheres = 34). Finally, the bump filter was modified. This filter is generally used to eliminate ligands which have too many atoms overlapping with the receptor. In addition to using the bump filter in the standard way, the bump grid in this application was modified to filter out molecules that had atoms extending out of the active site into the solvent.

Similarity and Superstructure Searches. A set of potential binding mode models was proposed by running DOCK on the initial inhibitors from this study and saving multiple orientations per compound. In some cases, potential binding modes were further refined with steepest descent and conjugate gradient minimization using the TRIPOS force field in Sybyl 6.2 (*12*). Superstructure and similarity searches of the ACD were used to identify a large set of compounds which were chemically similar to the inhibitors found in the initial DOCK screen (*17*, *18*). These searches were carried out with Daylight's Merlin system (*19*), using a Tanimoto similarity metric and Daylight's hashed connectivity fingerprints. We then assayed compounds from this set which tested specific aspects of our pharmacophore models. In general, compounds with conservative changes were selected.

Chemicals. All of the chemical compounds used in the enzyme assays were purchased from Sigma Chemical Co., the Sigma-Aldrich Library of Rare Chemicals (SALOR), Aldrich Chemical Co., Inc., Menai, or Maybridge. For the preliminary enzyme assays, [8-^{14}C]hypoxanthine (52 mCi/mmol) was from Moravek Biochemicals and [8-^{14}C]guanine (56 mCi/mmol) was obtained from ICN Radiochemicals. GMP, PRPP, pyrophosphate (PP$_i$), and the purine bases were purchased from Sigma Chemical Co. in the highest purity available.

Sources of Enzymes. Recombinant *T. foetus* HGXPRTase was purified to homogeneity from *Escherichia coli* strain SØ 606 transformed with the low-phosphate-inducible pBT-fprt expression plasmid (*4*). Recombinant human HGPRTase was purified from the same strain of *E. coli* transformed with the pBAcprt expression plasmid by a previously described procedure (*20*).

Enzyme Assays. For preliminary testing of the computer-selected compounds, a radioactivity assay of HPRTase (using radiolabeled hypoxanthine as the substrate) or GPRTase (using radiolabeled guanine as the substrate) activity was employed (*21*). In the initial screen, each chemical compound was tested at 1 mM. Compounds exhibiting over 50% inhibition of the enzyme activity were titrated to lower concentrations for determination of the IC$_{50}$ values. Chemical samples were dissolved in dimethyl sulfoxide (DMSO) to a concentration of 10 mM and tested in assay solutions of no more than 10% DMSO, which has no effect on the enzyme activity. For kinetic analysis of the enzyme-catalyzed reactions, a spectrophotometric assay was performed as previously described (*22*).

Kinetic Analysis. Data on the initial rate of the enzyme-catalyzed reaction were fitted to eqs 1−3 using kinetics analysis software and plotted on the basis of weight-based linear regression analysis (*23*, *24*).

For competitive inhibition

$$v = V_{max}S/[K_m(1 + I/K_{is}) + S]\qquad(1)$$

For noncompetitive inhibition

$$v = V_{max}S/[K_m(1 + I/K_{is}) + S(1 + I/K_{ii})]\qquad(2)$$

For uncompetitive inhibition

$$v = V_{max}S/[K_m + S(1 + I/K_{ii})]\qquad(3)$$

The best fit was determined in each case by the relative fit error and errors in the constants. The nomenclature is that of Cleland (*25*): v, initial velocity; V_{max}, maximum velocity; S, substrate concentration; K_m, apparent Michaelis constant; K_{is} and K_{ii}, slope and intercept inhibition constants, respectively; and I, inhibitor concentration.

In Vitro T. foetus Cell Culture. *T. foetus* kv1 strain trophozoites were cultivated to midlogarithmic phase in Diamond's TYM medium at 37 °C (*26*) and inoculated into fresh medium at a 10-fold dilution with resumption of the incubation. Time samples were taken, and the cell number in each sample was determined using a hemocytometer under a microscope. The concentration of DMSO in the culture

medium was maintained at or below 1% to avoid any adverse effect on cell growth.

RESULTS AND DISCUSSION

Active Site of T. foetus HGXPRTase. Figure 1A shows the active site of *T. foetus* HGXPRTase with bound GMP. The phosphate, ribose, and purine base moieties of the bound GMP interact with the protein through a network of hydrogen bonds. In addition, the purine base is inserted into a hydrophobic pocket, formed on one side by Tyr 156 and on the other side by Phe 162 and Ile 104. The active site of HGXPRTase extends beyond the region where the GMP is bound and includes a loop formed by residues 46−49. This loop appears to interact with pyrophosphate (*27*).

Somoza et al. (*8*) provided a detailed comparison of the active site of *T. foetus* HGXPRTase with that of human HGPRTase. This comparison revealed significant differences between the two active sites in the region that interacts with the C2 substituent of the purine base. Differences in this region were expected because the parasite and mammalian enzymes have different substrate specificities. The parasite enzyme accepts hypoxanthine, guanine, and xanthine as substrates with similar K_m values (*28*), while the mammalian enzyme accepts only hypoxanthine and guanine as substrates (*29*). The only difference between these three purine bases lies in the identity of the C2 substituent.

Using the Structural Information To Identify Potential HGXPRTase Inhibitors. The docking algorithm of Kuntz and co-workers (*13−15*) was used to screen the ACD for compounds showing van der Waals and electrostatic complementarity with the active site of *T. foetus* HGXPRTase. Since the HGXPRTase active site is large and shallow (approximately 10 Å × 10 Å × 5 Å), we focused primarily on the region encompassing the GMP binding site. This region is well-defined by the electron density map and differs from the corresponding region of the human HGPRTase.

On the basis of our computational screen, we assayed 18 chemical compounds for their ability to inhibit *T. foetus* HGXPRTase in vitro. The two most active compounds from this initial screen are shown at the top of Table 1 (**1** and **2**). These structures contain an indol-2-one (isatin) and a phthalic anhydride nucleus, respectively, each attached to a nitro-substituted benzene ring. Our modeling results led us to hypothesize that the indol-2-one (Figure 1B) and the phthalic anhydride (Figure 1C) fill the guanine binding pocket, while the nitrobenzenes fill a hydrophobic groove near the ribose phosphate binding loop of HGXPRTase. This hypothesis predicts competitive enzyme inhibition against guanine and GMP by these two compounds, which was verified in subsequent studies (see below). However, the precise mode of their bindings to the active site will have to be demonstrated by further structural analysis.

To improve the potency, selectivity, and aqueous solubility of the inhibitors, we used superstructure and similarity searches of the ACD to identify compounds which were chemically similar to the two initial inhibitors (**1** and **2** in Table 1). In the isatin series, we attempted to identify compounds with single changes in either the isatin moiety, the aromatic ring substituents, or the linker. In the phthalic anhydride series, we attempted to identify compounds with single changes in either the anyhydride, the aromatic ring
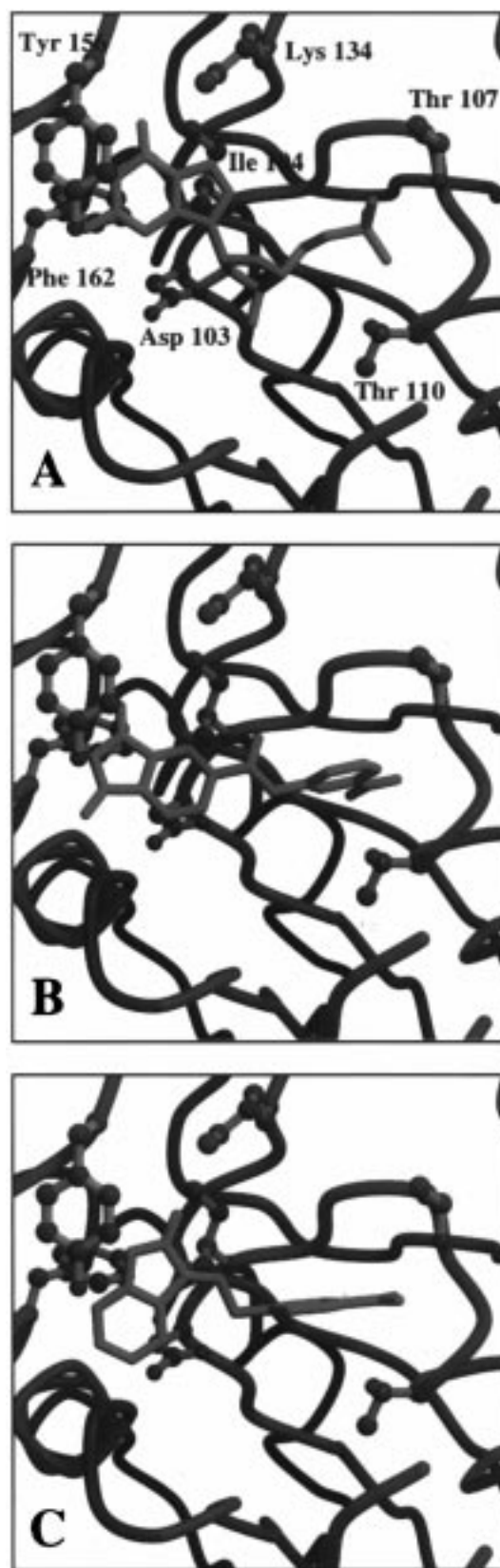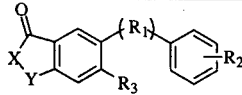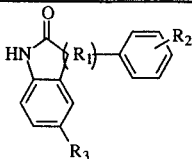

FIGURE 1: Active site of *T. foetus* HGXPRTase based on the crystal structure of this enzyme (*8*). Panel A shows the bound GMP as seen in the crystal structure. Panels B and C show the results of our modeling of the phthalic anhydride (Table 1, compound **1**) (B) and the indol-2-one (isatin) (Table 1, compound **2**) (C) in the active site of *T. foetus* HGXPRTase. The side chains that are shown are those that interact directly with the GMP. Our modeling suggests that the nitrobenzene moiety of each ligand interacts with Ile 105, Ile 109, and Met 111 (side chains not shown for clarity).

Table 1: Inhibition of *T. foetus* HGXPRTase (Tf) and Human HGPRTase (Hu) by the Indol-2-one (isatin) (right) and Phthalic Anhydride (left) Analog Series[a]

Cpd	X	Y	R1	R2	R3	Tf IC$_{50}$(μM)	Hu IC$_{50}$(μM)	Cpd	R1	R2	R3	Tf IC$_{50}$(μM)	Hu IC$_{50}$(μM)
1	O	C=O	C(=O)NH	3-NO$_2$	H	300	>1000	2	C=NN	p-NO$_2$	H	240	200
3	O	C=O	SCH$_2$	4-Cl	NO$_2$	425	>1000	10	C=NN=CH	2-OH,5-Br	H	460	>1000
4	O	CH$_2$	HNC=O	4-Cl	H	380	>1000	11	C=NNC(=O)C H$_2$	3,4-diOCH$_3$	Br	320	>1000
5	O	C=O	C(=O)NH	4-NHC(=O)C	H	140	>1000	12	C=NN=CH	3,4-diCl	Br	300	>1000
6	O	C=O	C(=O)NH	2,4-diCl	H	80	>1000	13	C=C(CH$_3$)CH$_2$CH$_2$	p-OCH$_3$	H	200	>1000
7	O	C=O	C(=O)NH	2-OCH$_3$,5-NO$_2$	H	70	>1000	14	C=NNC(=O)CH$_2$O	p-NO$_2$	H	180	>1000
8-TF1	O	C=O	C(=O)NH	3,4-diCl	H	50	>1000	15	C=NNC(=O)CH(CH$_3$)O	2,4-diCl	Br	85	>1000
9	O	C=O	C(=O)NH	2-OCH$_3$,5-Cl	H	22	>1000	16	C=NN=CH	p-Cl	H	10-75	>1000
								17	C=NN=CH	p-NO$_2$	H	50	>1000

[a] The two active chemical compounds that arose directly from the docking screen are shown at the top of Table 1 as compounds **1** and **2**. The remaining 16 inactive compounds from the docking screen that showed no effect on *T. foetus* HGPRTase up to 1 mM are as follows: acycloguanosine, phenolphthalein monophosphate di(cyclohexylammonium) salt, periodate-oxidized, borohydride-reduced guanosine, and 2',3'-O-p-anisylideneguanosine (from Sigma); 2-(3-carboxy-4-hydroxyphenyl)quinoline-4-carboxylic acid, 4,6-phenoxanthinedicarboxylic acid, 2-amino-6-benzylthiopurine, 5-amino-3-(4-bromophenyl)-4-oxothieno(3,4-D)pyridineazine-1-carboxylic acid ethyl ester, 2-(5-nitro-2-benzimidazolylimino)-4,5-imidazolidinedione, and 4'-methyl-3'-nitrosuccinanilic acid (from Salor); and 2-[1,2,4-triazolo(3,4-C)-1,2,4-benzotriazin-1-ylsulfanyl]acetic acid, 2-[(carboxyethyl)sulfanyl]-benzoic acid, 4-[(anilinocarbothionyl)oxy]-2-oxo-1,2-dihydroquinoline, 5-fluoro-2-(2-hydroxy-5-nitrophenyl)-2,3-dihydro-4(1H)-quinazolinone, O-3-[(6-chloro-3-carbonyl)pyridyl]-5-methyl-3-isoxazolecarbohydroximamide, and 2-{[3-amino-4-oxo-4H-1,3,4-thiadiazolo(2,3-C)-1,2,4-triazin-7-yl-]sulfanylacetic acid (from Maybridge).

substituents, or the linker. From this set of potential inhibitors, we assayed 22 compounds, which, according to our proposed pharmacophore, explored different regions of the HGXPRTase binding site. Eighteen (82%) of these 22 compounds had IC$_{50}$s below the 1 mM screening threshold, and 10 (45%) inhibited HGXPRTase with a potency equal to or higher than those of the two original inhibitors. The best compounds demonstrate IC$_{50}$s that are more than 1 order of magnitude lower than those of the lead compounds (Table 1). Furthermore, several of these compounds showed significantly more potent inhibition of the parasite HGX-PRTase than of the mammalian HGPRTase (Table 1).

We chose one of the compounds shown in Table 1 for further characterization. 4-[*N*-(3,4-Dichlorophenyl)carbamoyl]phthalic anhydride (compound **8**, referred to as TF1) was selected because it was one of the more potent inhibitors of the *T. foetus* HGXPRTase (IC$_{50}$ = 50 μM). Furthermore, it did not inhibit human HGPRTase in our screen (IC$_{50}$ > 1 mM), and it is sufficiently soluble in aqueous media to allow further testings in vitro.

A steady-state kinetic analysis using eqs 1−3 as described above showed that TF1 is a competitive inhibitor of guanine in the forward reaction, with a K_i of 13 μM, as well as a competitive inhibitor of GMP in the reverse reaction, with a K_i of 10 μM (Figure 2). The residual errors for the fit of the data to the models for competitive, noncompetitive, and uncompetitive inhibition were 5.3×10^{-6}, 2.8×10^{-2}, and 1.8, respectively, for the forward reaction and 0.31, 14.8, and 2.6, respectively, for the reverse reaction. These results are consistent with the modeling results, which predicted that the compound would bind to a region of the active site that overlaps with the GMP binding site.

Having shown that TF1 is a competitive inhibitor of *T. foetus* HGXPRTase, we explored the effect of this compound
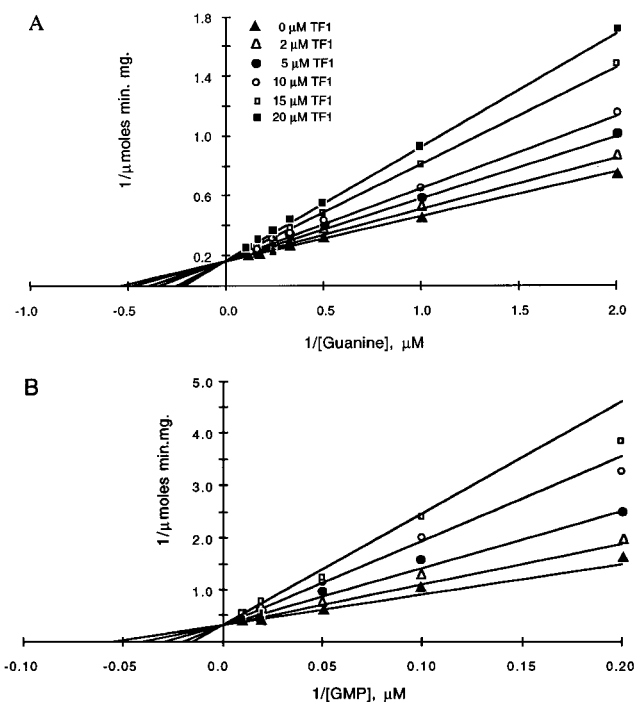

FIGURE 2: Kinetic data showing that 4-[*N*-(3,4-dichlorophenyl)-carbamoyl]phthalic anhydride (TF1) is a competitive inhibitor of guanine in the forward direction, with a K_i of 13.23 ± 2.03 μM (A), and a competitive inhibitor of GMP in the reverse direction, with a K_i of 9.97 ± 1.39 μM (B).

on the growth of *T. foetus* in in vitro culture. As shown in Figure 3, TF1 is a concentration-dependent inhibitor of *T. foetus* growth in culture with an EC$_{50}$ of approximately 40 μM. Furthermore, the inhibition of *T. foetus* growth by TF1 could be reversed by increasing the concentration of hypoxanthine in the growth medium (Figure 4). The growth
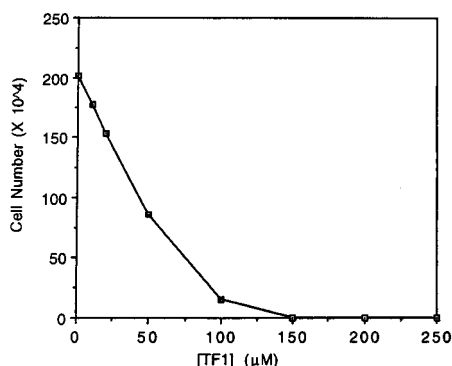
FIGURE 3: Data showing the effect of 4-[*N*-(3,4-dichlorophenyl)-carbamoyl]phthalic anhydride (TF1) on the in vitro growth of *T. foetus*. On the basis of these data, the EC_{50} of TF1 is estimated to be approximately 40 μM.
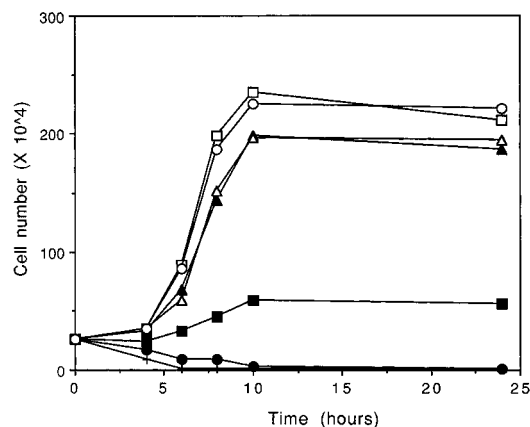

FIGURE 4: Data showing that the inhibition of 150 μM TF1 on the growth of *T. foetus* can be reversed by the addition of 1 mM exogenous hypoxanthine (Hx): (+) 0 Hx + 150 μM TF1, (●) 0.2 mM Hx + 150 μM TF1, (■) 0.5 mM Hx + 150 μM TF1, (▲) 1.0 mM Hx + 150 μM TF1, (△) 2.0 mM Hx + 150 μM TF1, (○) 2.0 mM Hx + 0 TF1, and (□) 0 Hx + 0 TF1. Exogenous guanine reverses the growth inhibition caused by TF1 in a similar manner (data not shown).

inhibition was also associated with decreased incorporation of exogenous radiolabeled guanine into the nucleic acid fraction of *T. foetus* (data not shown). Overall, these data support the conclusion that TF1 inhibits the growth of *T. foetus* in culture by functioning as a competitive inhibitor of the parasite's HGXPRTase.

Conclusion. We have identified two novel classes of non-purine analogue competitive inhibitors of a purine salvage enzyme. These inhibitors bind to the HGXPRTase approximately as well as any of the enzyme's natural substrates and inhibit the enzyme better than any other compound that has been found so far (*6*). The success of this project confirms the conclusions from our previous studies (*3*): that *T. foetus* HGXPRTase is a good target for antitritrichomonal drug design and that it is possible to use structure-based drug design to identify compounds that inhibit this enzyme but do not substantially inhibit the mammalian homolog. It is likely that the approach taken in this work will be broadly applicable to the design of other antimicrobials.

REFERENCES

1. Wang, C. C. (1984) *J. Med. Chem. 27*, 1−9.
2. Anderson, M. L., Barr, B. C., and Conrad, P. A. (1994) *Vet. Clin. North Am.: Food Anim. Pract. 10*, 439−461.
3. Wang, C. C., Verham, R., Rice, A., and Tzeng, S. F. (1983) *Mol. Biochem. Parasitol. 8*, 325−337.
4. Chin, M. S., and Wang, C. C. (1994) *Mol. Biochem. Parasitol. 63*, 221−229.
5. Sege-Peterson, K., Chambers, J., Page, T., Jones, O. W., and Nyhan, W. L. (1992) *Hum. Mol. Genet. 1*, 427−432.
6. Jadhav, A. L., Townsend, L. B., and Nelson, J. A. (1979) *Biochem. Pharmacol. 28*, 1057−1062.
7. Eads, J. C., Scapin, G., Xu, Y., Grubmeyer, C., and Sacchettini, J. C. (1994) *Cell 78*, 325−334.
8. Somoza, J. R., Chin, M. S., Focia, P. J., Wang, C. C., and Fletterick, R. J. (1996) *Biochemistry 35*, 7032−7040.
9. Jones, T. A., Zou, J. Y., Cowan, S. W., and Kjeldgaard, M. (1991) *Acta Crystallogr. A47*, 110−119.
10. *Insight II*, version 2.3.0 (1995) Biosym Technologies, San Diego, CA.
11. Ferrin, T. E., Huang, C. C., Jarvis, L. E., and Langridge, R. (1988) *J. Mol. Graphics 6*, 13−27.
12. *Sybyl*, version 6.2 (1995) Tripos Associates, St. Louis, MO.
13. Kuntz, I. D., Blaney, J. M., Oatley, S. J., Langridge, R., and Ferrin, T. (1982) *J. Mol. Biol. 161*, 269−288.
14. Meng, E. C., Shoichet, B. K., and Kuntz, I. D. (1992) *J. Comput. Chem. 13*, 505−524.
15. Meng, E. C., Gschwend, D. A., Blaney, J. M., and Kuntz, I. D. (1993) *Proteins: Struct., Funct., Genet. 17*, 268−278.
16. *Available Chemicals Directory*, version 95.1 (1995) Molecular Design Limited Information Systems, San Leandro, CA.
17. Brown, R. D., and Martin, Y. C. (1997) *J. Chem. Inf. Comput. Sci. 37*, 1−9.
18. Matter, H. (1997) *J. Med. Chem. 40*, 1219−1229.
19. *Daylight*, version 4.42 (1996) Daylight Chemical Information Systems, Inc., Santa Fe, NM.
20. Kanaaneh, J., Craig, S. P., III, and Wang, C. C. (1994) *Eur. J. Biochem. 223*, 595−601.
21. Beck, J. T., and Wang, C. C. (1993) *Mol. Biochem. Parasitol. 60*, 187−194.
22. Yuan, L., Craig, S. P., McKerrow, J. H., and Wang, C. C. (1992) *Biochemistry 31*, 806−810.
23. *K-CAT*, version 1.0 (1989) Biometallics, Inc.
24. *KinetAsyst, Gauss−Newton Analysis*, version II (1991) IntelliKinetics, State College, PA.
25. Cleland, W. W. (1963) *Biochim. Biophys. Acta 67*, 104−137.
26. Wang, A. L., and Wang, C. C. (1985) *Mol. Biochem. Parasitol. 14*, 323−335.
27. Scapin, G., Ozturk, D. H., Grubmeyer, C., and Sacchettini, J. C. (1995) *Biochemistry 34*, 10744−10754.
28. Munagala, N. R., Chin, M. S., and Wang, C. C. (1998) *Biochemistry 37*, 4045−4051.
29. Xu, Y., Eads, J., Sacchettini, J. C., and Grubmeyer, C. (1997) *Biochemistry 36*, 3700−3712.
30. Ferrin, T. E., Huang, C. C., Jarvis, L. E., and Langridge, R. (1988) *J. Mol. Graphics 6*, 36−37.

BI973095Z